

# Effect of Anode Temperature on Hall Thruster Performance

Carl F. Book\* and Mitchell L. R. Walker†

Georgia Institute of Technology, Atlanta, Georgia 30332

DOI: 10.2514/1.48028

The effects of anode temperature on the performance of a 5-kW Hall-effect thruster are investigated. The performance characteristics of the P5 Hall-effect thruster are measured with and without active cooling of the anode. Thrust, ion current density, anode temperature, and cooling power are measured for discharge voltages between 100 and 500 V at xenon propellant flow rates of 4.97 and 10.0 mg/s. All experiments are performed in a 4 by 7 m stainless-steel vacuum chamber at pressures below  $2.4 \times 10^{-5}$  Torr corrected for xenon. At 100 V, 4.97 mg/s, cooling affects a 6.3% increase in anode efficiency and a 56% increase in thrust-to-power ( $T/P$ ). At 100 V, 10.0 mg/s, cooling affects a 2.0% increase in anode efficiency and a 7.5% increase in  $T/P$ . For both propellant flow rates, the cooled anode efficiency unexpectedly decreases as the discharge voltage increases, which leads to a maximum anode efficiency loss of 5.0 and 9.1% at 4.97 and 10.0 mg/s, respectively.

## Nomenclature

$A_w$	=	surface area of coolant tube inner wall, $m^2$
$c_p$	=	coolant specific heat capacity, $J\ kg^{-1}\ K^{-1}$
$D$	=	inner diameter of coolant tubing, m
$e$	=	elementary charge, C
$h$	=	coolant heat transfer coefficient, $W\ m^{-2}\ K^{-1}$
$IF_c$	=	ionization fraction with cooling
$IF_{uc}$	=	ionization fraction without cooling
$k$	=	Boltzmann's constant, $J\ K^{-1}$
$k_w$	=	coolant thermal conductivity, $W\ m^{-1}\ K^{-1}$
$L/D$	=	coolant tube length-to-diameter ratio
$m_e$	=	electron mass, kg
$m_0$	=	neutral atom mass, kg
$Nu$	=	Nusselt number
$n_e$	=	electron number density, $m^{-3}$
$n_0$	=	neutral number density, $m^{-3}$
$Pr$	=	Prandtl number
$q$	=	power extracted by coolant, W
$Q_0$	=	electron-neutral collision cross section, $m^2$
$Re$	=	Reynolds number
$T_{eV}$	=	electron energy, eV
$T_0$	=	neutral propellant temperature, K
$Z_c$	=	electron-neutral collision frequency, $s^{-1}$
$\Gamma$	=	axial flux of neutrals, $m^{-2}\ s^{-1}$
$\Delta T_w$	=	wall to bulk fluid temperature difference, K
$\eta_a$	=	anode efficiency
$\eta_b$	=	current utilization efficiency
$\eta_m$	=	mass utilization efficiency
$\eta_o$	=	utilization efficiency for discharge power
$\eta_T$	=	thruster efficiency
$\eta_v$	=	voltage utilization efficiency
$\lambda$	=	axial penetration distance, m
$\mu$	=	coolant dynamic viscosity, Pa s
$\langle\sigma_i v_e\rangle$	=	ionization reaction rate, $m^3\ s^{-1}$
$\bar{v}$	=	average neutral speed, $m\ s^{-1}$
$\bar{v}_{e0}$	=	average electron speed relative to neutrals, $m\ s^{-1}$

## Introduction

HALL-EFFECT thrusters (HETs) represent an effective alternative to chemical based rocket propulsion for low thrust applications in spacecraft. The high thrust-to-power ( $T/P$ ) regime of HET operation is well suited to orbit transfer for earth-orbiting satellites. Military and commercial satellite programs benefit from the savings in propellant mass fraction offered by this class of electric thruster [1]. There are many factors which determine the performance of a thruster, but in general propellant utilization is critical to efficient operation. Analysis of the neutral flow dynamics in HET discharge channels indicates that propellant utilization will improve as neutral residence time increases. Several studies have been performed, including reverse injection of propellant, the use of a shim anode, and propellant injection through the discharge channel walls [2]. The resultant increase in residence time is expected to yield an increase in ionization fraction, thereby increasing the thrust,  $T/P$  ratio, specific impulse, and efficiency. A cooled anode study performed by Wilbur and Brophy showed that the performance of an ion thruster can be improved through an increase in propellant residence time in the discharge chamber [3]. The results of this work lead to the reverse injection technique used in contemporary gridded ion engines.

The work contained herein seeks to increase HET neutral residence time through anode cooling. The thruster used throughout this study is the P5 HET. The P5 is a laboratory model Hall thruster with a mean anode diameter of 147 mm, a channel width of 25 mm, a channel depth of 38 mm, and a nominal power rating of 5 kW. More information on the P5 is available in [4]. The performance changes generated by the cooled anode, as well as the power extracted from the anode, are calculated for each operating condition. Power deposition to the anode is a prominent loss mechanism for HETs, and its severity will impact the anode temperature, which in turn affects neutral flow properties. The quantification of power loss to the anode will provide insight into HET operation. The anode temperature is recorded at each operating condition, and the temperature measurements are used to calibrate a thermal model of the anode. We begin with a discussion of first-order analytical modeling to understand the magnitude of the potential performance changes due to cooling. Subsequent thermal simulations guide the design of the cooled anode and facilitate the sizing of the coolant system. Experimental data are presented for the new anode with and without cooling enabled, and the changes in performance are discussed in terms of thrust, anode efficiency,  $T/P$  ratio, discharge current oscillations, ion current density, and electron-neutral collision frequency.

## First-Order Modeling

Changes in thruster performance due to cooling are estimated based on the ionization reaction rate and the flux of neutrals in the discharge channel. These estimates reveal that cooling is most

Received 7 November 2009; revision received 26 May 2010; accepted for publication 3 June 2010. Copyright © 2010 by Carl F. Book. Published by the American Institute of Aeronautics and Astronautics, Inc., with permission. Copies of this paper may be made for personal or internal use, on condition that the copier pay the \$10.00 per-copy fee to the Copyright Clearance Center, Inc., 222 Rosewood Drive, Danvers, MA 01923; include the code 0748-4658/10 and \$10.00 in correspondence with the CCC.

\*Graduate Research Assistant, Department of Aerospace Engineering, 270 Ferst Drive.

†Assistant Professor, High-Power Electric Propulsion Laboratory, Department of Aerospace Engineering, 270 Ferst Drive. Senior Member AIAA.

beneficial at low discharge voltage. The predicted improvements guide the design of the experiment and also serve to verify the experimental results. A brief exploration of propellant heating is followed by a description of the final cooling system. All thermal simulations are performed in COMSOL Multiphysics [5].

**Performance Estimates**

A review of Hall thruster physics assembled by Goebel and Katz provides an analytical expression for the average ionization reaction rate for plasmas within the temperature range  $10 \text{ eV} < T_{eV} < 40 \text{ eV}$  [6]:

$$\langle \sigma_i v_e \rangle = 10^{-20} \left[ -(1.031 \cdot 10^{-4}) T_{eV}^2 + 6.386 \exp\left(\frac{-12.127}{T_{eV}}\right) \right] \sqrt{\frac{8eT_{eV}}{\pi m_e}} \quad (1)$$

The neutral propellant particle speeds are assumed to obey a Maxwellian distribution. The average speed is

$$\bar{v} = \sqrt{\frac{8kT_0}{\pi m_0}} \quad (2)$$

The penetration distance represents the average distance traveled before ionization occurs:

$$\lambda = \frac{\bar{v}}{n_e \langle \sigma_i v_e \rangle} \quad (3)$$

An extension of the one-dimensional particle flux model yields an expression for the fraction of neutral particles which are ionized within a given axial distance from the anode [6]:

$$IF = \left[ 1 - \exp\left(\frac{-x}{\lambda}\right) \right] \quad (4)$$

This ionization fraction is a function of the neutral propellant temperature, plasma temperature, electron number density, and axial position relative to the anode exit plane. If  $x$  is taken to be the length of the ionization region then IF can be related to the mass utilization efficiency of the thruster. With separate cooled and uncooled ionization fractions, the change in mass utilization efficiency can be interpreted as

$$\Delta \eta_m = \frac{IF_c}{IF_{uc}} - 1 \quad (5)$$

which can be reduced to a function of only the cooled and uncooled propellant temperatures by substitution of the appropriate values for the plasma temperature, electron number density, and ionization region length. For the P5, the ionization region length is approximated as  $x \approx 12 \text{ mm}$  [7]. This value represents a nominal operating condition, and in the context of the performance estimate it is assumed, for simplicity, to be constant. Assuming a cathode efficiency of unity, the change in mass utilization efficiency is used to estimate the change in total efficiency:

$$\eta_T = \eta_a \eta_o \quad (6)$$

The anode efficiency can be expressed as the product of the mass, current, and voltage utilization efficiencies, denoted by subscripts  $m$ ,  $b$ , and  $v$ , respectively:

$$\eta_a = \eta_m \eta_b \eta_v \quad (7)$$

Experiments show that  $\eta_o \approx 0.92$ ,  $\eta_v \approx 0.90$ , and  $\eta_b \approx 0.75$  for the P5 [8]. Neglecting multiple ionization, the total efficiency for the device is given in Eq. (8):

$$\eta_T \approx 0.62 \eta_m \quad (8)$$

Thus, it is assumed that the change in thruster efficiency due to cooling equals the change in mass utilization efficiency multiplied by a factor of 0.62. With the ratio of cooled-to-uncooled anode temperatures estimated from heat transfer simulations, the predicted change in total efficiency due to cooling is presented as a function of electron number density and electron temperature in Fig. 1. Cooling the propellant increases the fraction of propellant atoms that are ionized. The effect of cooling is more pronounced at low electron number density and temperature because the fraction of the electron population with sufficient energy to ionize propellant is small under such conditions. Enhanced residence time gives the high energy component of the electron population more time to ionize neutrals before they exit the thruster. From the plasma potential measurements in [7] it is known that electron temperature decreases with discharge voltage. Since the high  $T/P$  operating regime is achieved at below-nominal discharge voltages, cooling will be most effective when operating at high  $T/P$ . The estimated change in total efficiency for a thruster with a nominal 30 eV electron temperature and a density of  $5 \times 10^{17} \text{ m}^{-3}$  is 2.8%.

**Neutral Propellant Temperature**

Thermal simulations are performed to estimate the change in anode temperature due to cooling. The simulations are also used to determine the temperature of the front faces of the P5 anode based on extrapolations of the temperature measured on the rear of the anode. Figure 2 shows a diagram of the P5 anode.

Reid demonstrates that propellant gas inside a HET anode will adjust rapidly to the anode body temperature [1]. A thermal model in [9] is used to estimate the power deposited on the anode due to collisions with electrons at an electron temperature and discharge current of 15 eV and 13 A, respectively. The result is approximately 500 W. This model does not account for radiative heating of the anode, which is much more difficult to estimate than collisional heating. In an effort to consider radiative heating, it is assumed that the total power deposition to the anode will be as high as 1 kW at the nominal 5 kW operating condition. The first simulation evaluates the temperature profile of the P5 anode exposed to a 1 kW heat flux. It is not necessary to model the entire thruster because the thermal conductivities of stainless-steel and boron nitride (BN) are low ( $\sim 25 \text{ W/m-K}$  for stainless-steel and BN compared with

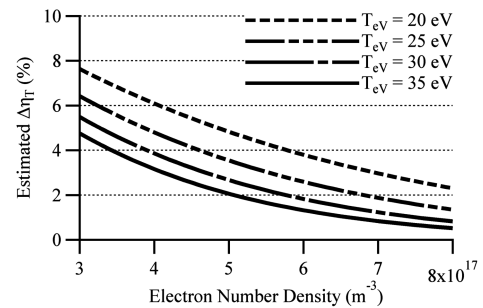


Fig. 1 Estimated change in thruster efficiency due to cooling as a function of electron number density and temperature.

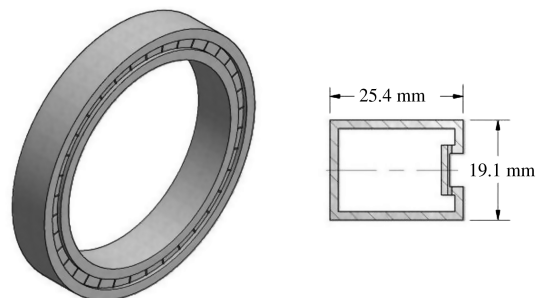


Fig. 2 Full and cross sectional views of original P5 anode.

400 W/m-K for copper). This means that heat conduction between the anode and the discharge channel is small compared with the heat flux from the plasma to the anode. Therefore, the anode temperature can be simulated to first order without consideration of other thruster components. The heat flux, which is assumed to be uniform, is modeled as a boundary condition on the anode faces directly exposed to the plasma. In practice, the heat flux to the anode in any HET is not necessarily uniform, however, the degree of nonuniformity is not known and likely varies with the operating condition. Thus, the nonuniformities in the heat flux to the anode are neglected in the thermal model. Radiative heat loss is permitted, and the material properties are set to match 316 stainless steel. Figure 3 shows that the anode faces exposed to the heat flux are much hotter than the surrounding anode body, which is a result of the low thermal conductivity of stainless steel. The simulated temperature at the anode exit is slightly less than 1000 K, which is consistent with simulations performed for a similar thruster, the NASA-173M [2].

To maximize cooling effectiveness it is desirable to place the coolant lines as close as possible to the anode exit plane without obstructing the exit plane orifices. The final cooling system design implements a 0.25 in.-outer-diam copper tube inside the anode. Figure 4 shows the coolant tubing, the corresponding circular groove in the new anode body, and an internal view of the anode partially assembled.

The body of the new P5 anode has the same external geometry and orifice arrangement as the original P5 anode. The internal geometry differs due only to the slot added for the coolant tubing. The tubing is held in place with a stainless-steel ring featuring a matching 0.25 in.-diam semicircular groove. The ring is pressed into place with rods supported by the back wall of the anode. Figure 4 shows the copper spacer that occupies the gap between the bends in the tubing. This spacer facilitates heat transfer away from the anode in the small region where the cooling tube does not contact the anode surface.

Figure 5 shows that the simulated wall temperature of the cooled anode is approximately 618 K. The simulation boundary conditions are identical to the uncooled simulation, except for the addition of cooling which is modeled as a heat flux through the inner walls of the tubing. The contact resistance between the copper tubing and anode body is assumed to be small due to the large contact pressure created by the ring and rods, and is thus neglected in the simulation. It is assumed that the cooling system would be capable of extracting up to 1 kW of power from the anode.

The simulation indicates that an extraction of 1 kW of thermal power yields 475 K on the inner walls of the copper tubing. Before

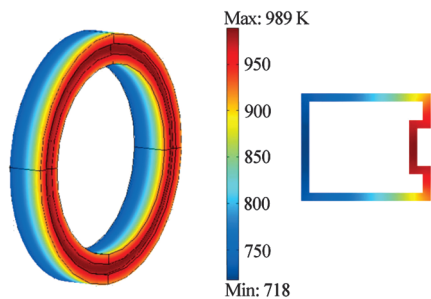


Fig. 3 Simulated temperature profile of uncooled P5 anode subjected to 1 kW heat flux on front faces.

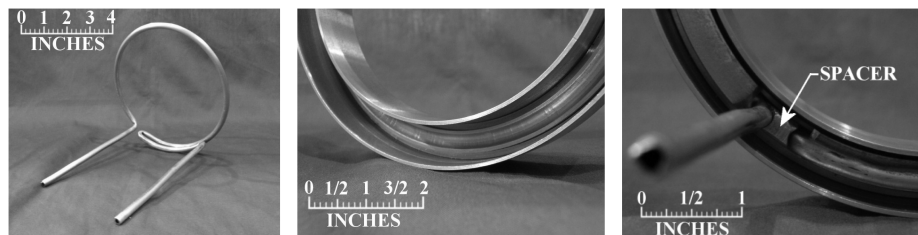


Fig. 4 Coolant tubing, internal view of anode body, and partial assembly showing copper spacer.

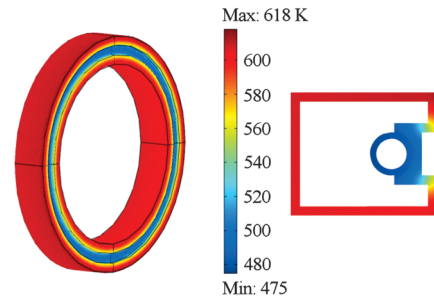


Fig. 5 Simulation results for cooled anode with 1 kW power deposition on front faces.

using this result in the performance model, it must be verified that the coolant can absorb 1 kW of thermal power from the copper tubing at this temperature. The experiment uses 3M Fluorinert FC-3283 as the coolant, and the heat transfer coefficient of FC-3283 is estimated with the Dittus-Boelter (DB) correlation [10]. Equation (9) shows the DB correlation for fully-developed turbulent flow:

$$h = \frac{k_w}{D} Nu = \frac{k_w}{D} (0.023 \cdot Re^{0.8} \cdot Pr^{0.4}) \quad (9)$$

The assumption of fully-developed turbulent flow requires that the tube length-to-diameter ratio,  $L/D$ , exceeds 60. In this experiment  $L/D > 400$ . The DB correlation requires  $Re > 10,000$  and  $0.7 < Pr < 100$ . Material properties for the tube and coolant are available in their respective datasheets. For this calculation,  $D = 0.18$  in.,  $k_w = 0.066$  W/m-K,  $\mu = 0.0014$  Pa-s, and  $c_p = 1100$  J/kg-K. The tube inner diameter is known within a manufacturing tolerance of 0.01 in.; however, the diameter will change slightly during bending. The exact amount of deformation is not known, however, the radius of curvature of the main arc is much larger than the tube diameter. Thus, the deformation will be small and the actual heat transfer coefficient should agree well with the value calculated herein. Taking the tube inner diameter as the characteristic length in the Reynolds number and assuming a mass flow rate of 0.12 kg/s ( $\sim 1$  gpm for FC-3283) yields  $Re = 23,900$  and  $Pr = 23.3$ . The heat transfer coefficient is 3700 W/m<sup>2</sup>K. The difference between the bulk fluid temperature and the tube inner wall temperature is given by Eq. (10):

$$\Delta T_w = \frac{q}{A_w \cdot h} \quad (10)$$

For the cooled anode,  $\Delta T_w$  is 41 K. In addition to the radial temperature gradient in the tube, coolant flowing at 0.12 kg/s will experience a bulk temperature rise of about 9 K inside the anode. If the coolant enters the anode at 283 K, a wall temperature of at least 333 K is required to facilitate the transfer of 1 kW of heat to the coolant, which is well below the simulation result of 475 K. Although the DB correlation is merely an estimate, the simulated temperature substantially exceeds the estimated 333 K lower limit, indicating that the uncertainty in the DB correlation is not sufficient to warrant dismissal of the simulation results. The simulation is therefore acceptable for use in the performance model. From the strong relationship between anode temperature and neutral propellant temperature, the simulation results from Fig. 3 and 5 are used to estimate the change in propellant temperature based on cooling. The

uncooled propellant temperature is assumed to be 920 K due to the hot front faces, and the cooled propellant temperature is assumed to be 610 K. The ratio of cooled-to-uncooled propellant temperatures is 0.66, which allows us to estimate the change in thruster efficiency as described in the previous section.

## Experimental Apparatus and Results

### Vacuum Facility

All tests on the cooled P5 anode are performed in the vacuum test facility (VTF). The VTF is a stainless-steel vacuum chamber that has a diameter of 4 m and a length of 7 m. Two 3800 CFM blowers and two 495 CFM rotary-vane pumps evacuate the facility to moderate vacuum (30 mTorr). To reach high-vacuum ( $10^{-7}$  Torr), the VTF employs six 48 in. diffusion pumps with a combined nominal pumping speed of 600,000 l/s on air, 840,000 l/s on hydrogen, and 155,000 l/s on xenon. The facility base pressure is  $1.2 \times 10^{-4}$  Pa ( $9.5 \times 10^{-7}$  Torr). VTF pumping speed is varied by changing the number of diffusion pumps in operation, and facility pressure is measured using a Varian 571 series ion gauge. High-purity (99.9995% pure) xenon propellant is supplied to the thruster and cathode through stainless-steel feed lines. MKS 1179JA mass flow controllers meter the anode and cathode propellant flow. The flow controllers are calibrated with a custom apparatus that measures gas pressure and temperature as a function of time in an evacuated chamber of known volume. The mass flow controllers have an accuracy of  $\pm 1\%$  full scale. A reproduction Moscow Aviation lanthanum hexaboride ( $\text{LaB}_6$ ) cathode is used for all tests. Electrical connections enter the chamber through separate feed-through ports, and the thruster discharge supply implements a filter consisting of a  $1.3\Omega$  resistor in series with the discharge current and a  $95 \mu\text{F}$  capacitor in parallel. The filter damps the low frequency discharge oscillations associated with the breathing mode of the thruster. Discharge current oscillations are measured with a F. W. Bell IHA-25 Hall probe connected to a Tektronix TDS 3034B oscilloscope. The discharge oscillations of the thruster in the cooled and uncooled anode configuration are measured over a 4 ms window at a sampling frequency of 2.5 MHz.

Figure 6 shows a schematic of the experiment setup. The P5 anode is cooled with a Neslab CFT 33 recirculating chiller and 3M Fluorinert FC-3283 coolant. Fluorinert FC-3283 is a specialty heat transfer fluid with a dielectric breakdown voltage of 43 kV across a

0.1 in. gap, thus it is well suited to cool the anode. An Omega FTB-902 liquid turbine flow meter with an FLSC-61 signal conditioner records the volumetric coolant flow rate within an uncertainty of  $\pm 0.5\%$  of the reading. Two Omega P-M series ultra precise resistance temperature detectors (RTD probes, uncertainty  $\pm 0.1^\circ\text{C}$ ) are installed in the coolant path to record the coolant temperature for use in calculating the power extracted from the anode. Two Omega type-K transition joint thermocouple probes are positioned on the rear of the anode, centered and diametrically opposed. The thermocouple uncertainty is  $\pm 1.1^\circ\text{C}$ . To prevent a short circuit and protect the data acquisition system, each thermocouple implements an Omega DRF-TCK voltage-isolating signal conditioner outside the VTF. The coolant and propellant lines are electrically isolated from the VTF and thrust stand with 0.25 in. Insulator Seal 6000 V cryogenic/liquid breaks, also known as cryobreaks. The thruster is mounted on a null-type inverted-pendulum thrust stand [11].

The current density profile of the plume is measured with a nude Faraday probe. The probe has a 2.22 cm-(0.875 in.)-diam collection electrode surrounded on the perimeter by a guard ring. Data is sampled every 0.45 deg as the probe sweeps continuously from  $-100$  to  $100$  deg relative to thruster centerline. The radius of the sweep is 1.0 m, and the probe accelerates to the input angular speed ( $3 \text{ deg/s}$ ) within the first 5 deg of rotation. The collection electrode is aluminum that is spray-coated with tungsten to minimize secondary electron emission. The collector and guard ring are biased to the same negative potential below facility ground. Biasing the guard ring and collector to the same potential minimizes edge effects around the collector by creating a flat, uniform sheath over the collection area. The electrical schematic for the nude Faraday probe is available in [12].

All tests are performed at anode voltages from 100 to 500 V and xenon flow rates of 4.97 and 10.0 mg/s. The cooled and uncooled operating conditions use the same mass flow rates, discharge voltages, and inner and outer magnetic currents. This ensures that the differences in performance observed between the two tests are due only to the use of the cooling system. Table 1 summarizes the operating parameters of the thruster with and without anode cooling. With the new anode in the uncooled configuration, the performance of the thruster is consistent with historical data for the P5 [4]. All differences are attributed to manufacturing tolerances and facility effects such as backpressure, choice of cathode, and instrument uncertainties.

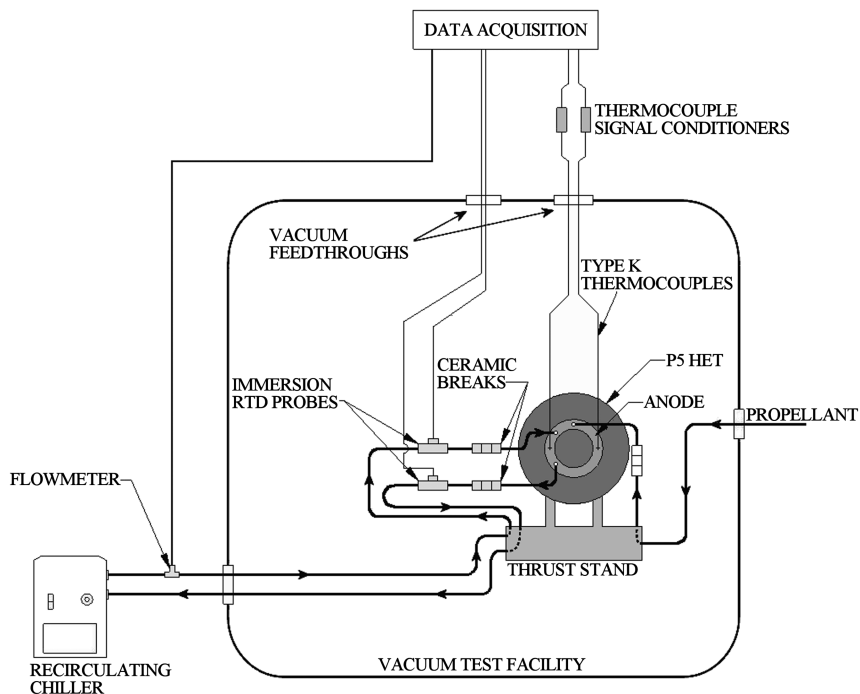


Fig. 6 Schematic of cooled P5 anode experimental setup, thermocouple positions on anode are accurate.

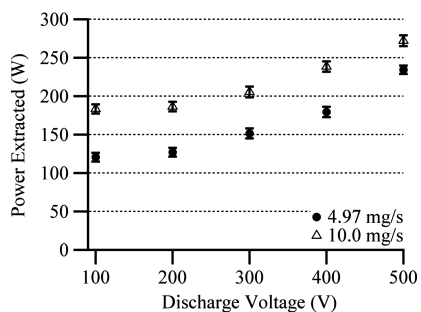
**Table 1 Summary of Cooled and Uncooled P5 Performance Data**

Cooled and uncooled					Cooled only			Uncooled only		
Discharge voltage, V	Anode flow, mg/s	Cathode flow, mg/s	Inner mag current, A	Outer mag current, A	Discharge current, A	Discharge power, W	Operating pressure, Torr-Xe	Discharge current, A	Discharge power, W	Operating pressure, Torr-Xe
100	4.97	1.01	4.1	4.7	5.7	570	$1.7 \times 10^{-5}$	4.4	440	$1.8 \times 10^{-5}$
200	4.97	1.01	1.4	1.3	5.3	1060	$1.7 \times 10^{-5}$	5.2	1040	$1.8 \times 10^{-5}$
300	4.97	1.01	2.3	1.9	5.7	1710	$1.7 \times 10^{-5}$	5.4	1620	$1.8 \times 10^{-5}$
400	4.97	1.01	1.2	3.8	5.8	2320	$1.7 \times 10^{-5}$	5.5	2200	$1.8 \times 10^{-5}$
500	4.97	1.01	5.0	10.2	7.2	3600	$1.7 \times 10^{-5}$	7.3	3650	$1.8 \times 10^{-5}$
100	10.0	1.01	3.0	2.9	14.3	1430	$2.3 \times 10^{-5}$	14.6	1460	$2.4 \times 10^{-5}$
200	10.0	1.01	2.7	1.8	11.7	2340	$2.3 \times 10^{-5}$	11.7	2340	$2.4 \times 10^{-5}$
300	10.0	1.01	3.5	2.7	11.6	3480	$2.3 \times 10^{-5}$	11.1	3330	$2.4 \times 10^{-5}$
400	10.0	1.01	3.5	4.1	12.1	4840	$2.3 \times 10^{-5}$	11.8	4720	$2.4 \times 10^{-5}$
500	10.0	1.01	4.2	5.8	12.8	6400	$2.3 \times 10^{-5}$	12.2	6100	$2.4 \times 10^{-5}$

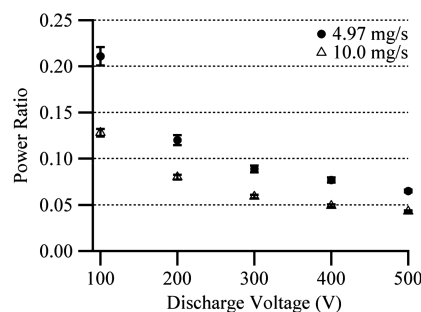
**Power Extraction and Cooling Effectiveness**

The cooling system is verified through several thermal soakback tests in the VTF. Before, during, and after thruster operation, thermocouples record the temperature of the RTD probe housing and the tubing both upstream and downstream of the probe housing. The downstream thermocouple is placed several feet downstream of the thruster so that the stainless-steel tubing will conduct very little heat from the anode to the downstream thermocouple. The test is considered successful if the thermocouple on the RTD probe housing reads within 0.2°C of the downstream thermocouple. In this experiment, 0.2°C is close to the thermocouple uncertainty. A successful test indicates that the heat from the anode is not appreciably soaking back to the RTD probe, thereby corrupting the coolant temperature measurement. Thermal soakback to the RTD probes is eliminated by adding approximately 1 ft of 316 stainless-steel tubing between the cryobreaks and RTD probes. Thruster performance data are not recorded during the soakback tests. Figure 7a shows the power extracted from the anode at each operating condition, and Fig. 7b shows the power ratio (extracted power-to-discharge power).

The ratio of extracted power-to-discharge power increases with decreasing discharge voltage, which reveals that power deposition to



**a) Power extracted from cooled anode**



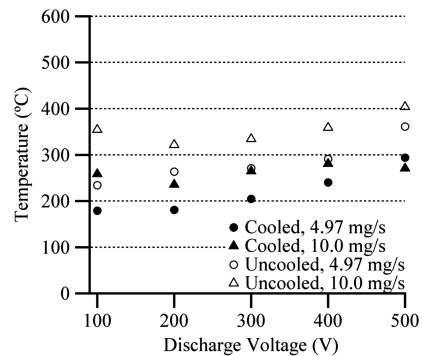
**b) Ratio of extracted power to discharge power**

**Fig. 7 Power extraction from anode during cooled testing as a function of discharge voltage at 4.97 and 10.0 mg/s.**

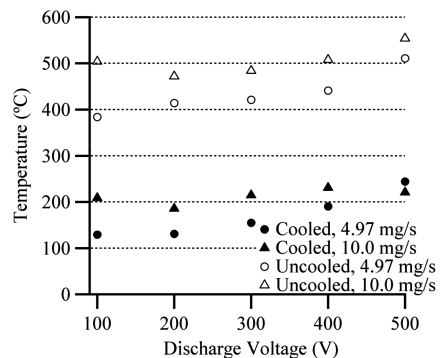
the anode is a prominent loss mechanism in the high  $T/P$  regime. Figure 8 shows the changes in anode temperature due to cooling. The values in Fig. 8 are calculated by averaging the readings from the two thermocouples for each operating condition. Note that the probe type thermocouples used for these measurements are sandwiched between the rear of the anode and the discharge channel. The dip at 500 V, 10 mg/s, with cooling is due to the failure of one of the thermocouples. The cooled anode is designed to extract power near its exit plane where anodes are typically hottest, thus the temperature change at the exit plane will be much larger than at the rear of the anode where the thermocouples reside. The simulation results in Fig. 3 and 5 are used to estimate the average temperature at the front (exit plane) of the anode.

**Thrust**

Figure 9 shows that the thrust is slightly higher for the cooled tests at 100 V, but as the discharge voltage is increased the uncooled anode proves superior. The same trend is also present in the  $T/P$  ratios

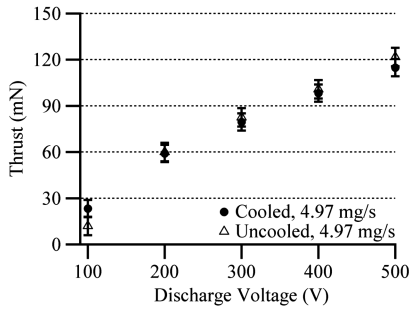


**a) Measured anode rear temperatures**

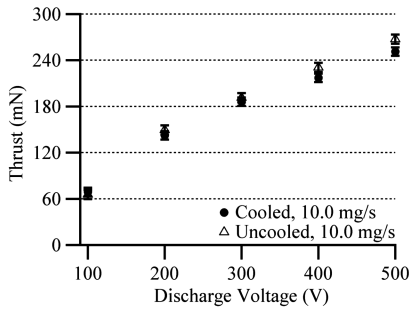


**b) Projected exit plane temperatures**

**Fig. 8 Anode temperature as a function of discharge voltage at 4.97 and 10.0 mg/s in the cooled and uncooled configurations.**



a) Thrust comparison at 4.97 mg/s



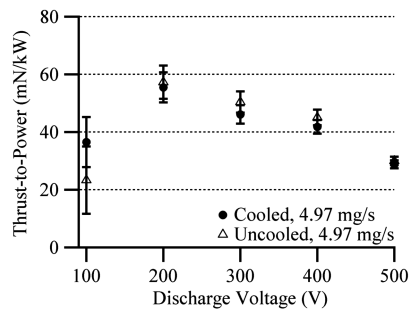
b) Thrust comparison at 10.0 mg/s

Fig. 9 Thrust as a function of discharge voltage at 4.97 and 10.0 mg/s in the cooled and uncooled configurations.

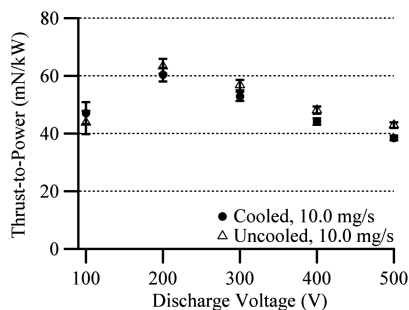
plotted in Fig. 10. For several data points, the apparent effect of cooling lies within the experimental uncertainty.

**Efficiency**

Anode efficiency is calculated as a function of thrust, propellant flow rate, and discharge power. The propellant flow rate is controlled during testing, therefore the trends in thrust and discharge power drive the trend in anode efficiency. Figure 11 contains anode efficiencies for the cooled and uncooled tests at both mass flow rates.

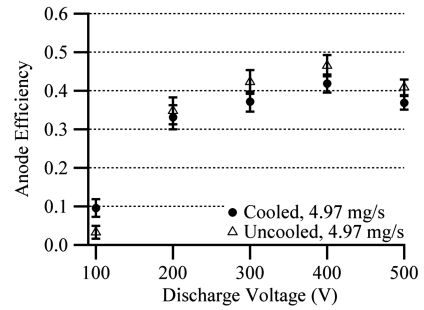


a) T/P comparison at 4.97 mg/s

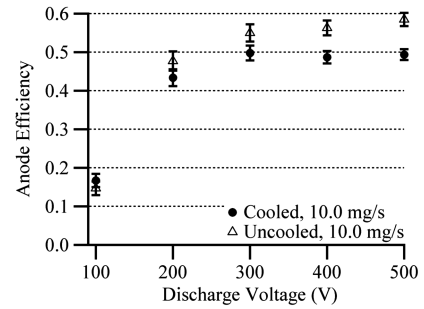


b) T/P comparison at 10.0 mg/s

Fig. 10 T/P as a function of discharge voltage at 4.97 and 10.0 mg/s in the cooled and uncooled configurations.



a) Anode efficiencies at 4.97 mg/s



b) Anode efficiencies at 10.0 mg/s

Fig. 11 Anode efficiency as a function of discharge voltage at 4.97 and 10.0 mg/s in the cooled and uncooled configurations.

At 100 V, the cooled thruster is more efficient for both propellant flow rates. Recall that the modeling described above predicts that the improvement in efficiency due to cooling is most pronounced at low discharge voltage. Experimentally, as the anode voltage is increased the benefits of cooling give way to other effects that cause the uncooled efficiency to overtake the cooled efficiency. These effects will be addressed in the Discussion section below. At every operating condition above 200 V, the uncooled anode efficiency exceeds the cooled anode efficiency by an amount greater than the experimental uncertainty.

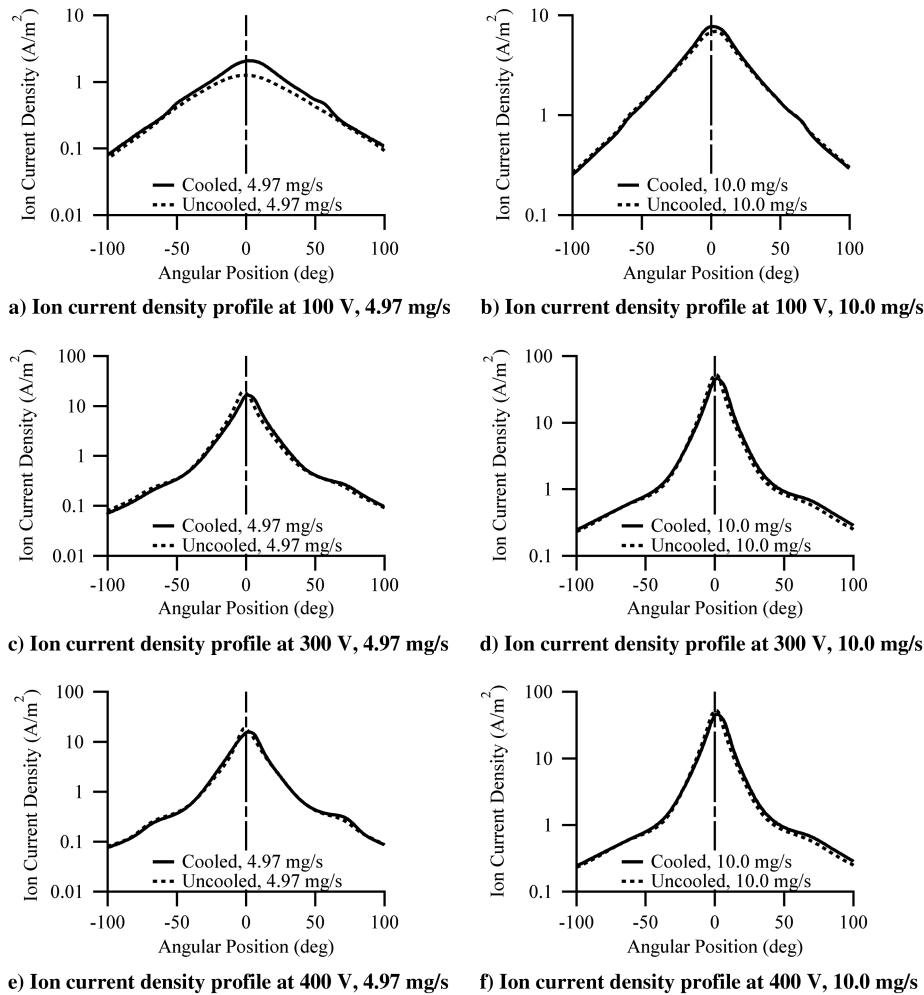
**Nude Faraday Probe Data**

Figure 12 shows several representative ion current density profiles. At 100 V, the peak current density with cooling exceeds the peak current density without cooling by 66% (at 4.97 mg/s) and 12% (at 10.0 mg/s). There is a 5.1% experimental uncertainty in the peak current density measurements at 100 V. As the discharge voltage increases, the cooled beam maximum shifts off centerline by an average of 1.75 deg in the positive angular direction. This direction corresponds to the location of the propellant inlet tube. The uncertainty in the probe position is  $\pm 1.27$  deg.

The total ion beam current is calculated by integrating the ion current density in spherical coordinates [12]. At large angles, the current density measured by the nude Faraday probe is strongly impacted by the presence of charge-exchange ions [13]. To examine potential differences in beam collimation between the cooled and uncooled tests, the fraction of the total ion current contained within  $\pm 30^\circ$  of thruster centerline is presented in Table 2. At 100 and 200 V, cooling the anode leads to an increase in the fraction of the ion current contained within  $\pm 30^\circ$  of thruster centerline, which is interpreted as an increase in beam collimation. Above 200 V, the differences between the cooled and uncooled tests fall within the measurement uncertainty of the Faraday probe and data acquisition system.

**Discharge Current Oscillations**

Figure 13 presents representative data for the discharge current oscillations measured for both the cooled and uncooled configurations. Time domain analysis illustrates a consistent increase in discharge current oscillation amplitude due to cooling. Power



**Fig. 12** Comparison of cooled and uncooled ion current density profiles at discharge voltages of 100, 300, and 400 V, and propellant flow rates of 4.97 and 10.0 mg/s.

spectral analysis reveals that the first breathing mode is dominant and usually occurs at frequencies between 15 and 20 kHz. At a fixed propellant mass flow rate, if the propellant is cooled within the anode then its number density will increase. If the increase in neutral density is maintained into the discharge channel, then each period of the breathing mode during cooling will produce a greater number of interactions between electrons and neutrals per unit volume. Near the anode, this produces a larger periodic electron flux to the anode hence larger discharge current oscillation amplitude. One would expect the breathing mode frequency to decrease with cooling, yet power spectral analysis does not reveal any discernible pattern in the frequency changes produced by cooling. By mass continuity, the expectation of lower breathing mode frequency is implicitly based on the assumption that the volume in which the plasma oscillation

occurs is constant. This assumption cannot be evaluated without measurement of the plasma properties at each operating condition.

### Discussion

The anode efficiency and centerline ion current density are increased by cooling the anode at 100 V. To explain the degradation of performance at higher discharge voltages, several factors must be addressed including the electron-neutral collision frequency, electron mobility, and plasma location inside the discharge channel. Cooling causes an increase in the electron-neutral collision frequency, which markedly improves ionization at low discharge voltage and also increases electron mobility. At 100 V the gain in ionization is sufficient to affect a net increase in efficiency. The gain

**Table 2** Fraction of ion beam current contained within  $\pm 30$  degrees of thruster centerline

Discharge voltage, V	Anode flow, mg/s	Cooled beam content, $\pm 30^\circ$ , %	Uncooled beam content, $\pm 30^\circ$ , %	Cooled vs uncooled, %	Uncertainty, %
100	4.97	36.3	32.4	3.9	1.1
200	4.97	63.4	60.9	2.5	2.1
300	4.97	63.0	62.8	0.2	2.0
400	4.97	63.2	61.6	1.6	2.0
500	4.97	57.8	57.4	0.4	1.8
100	10.0	39.5	37.4	2.1	1.2
200	10.0	62.2	60.0	2.2	1.9
300	10.0	62.9	63.5	-0.6	2.0
400	10.0	64.7	63.4	1.3	2.0
500	10.0	64.1	63.6	0.5	2.0

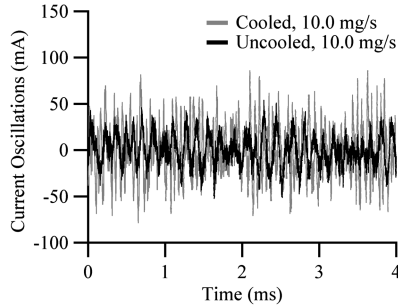


**Fig. 13** Discharge current oscillations at 200 V, 10.0 mg/s in the cooled and uncooled configurations.

in ionization due to cooling becomes negligible as the discharge voltage increases, yet electron mobility remains enhanced. Enhanced electron mobility leads to higher discharge current which, when coupled with an increased breathing mode amplitude and azimuthal nonuniformities in the propellant distribution causes the observed decrease in efficiency at discharge voltages above 100 V. Cooling is most beneficial in the high  $T/P$  regime where power deposition to the anode is a dominant loss mechanism.

### Collision Frequency

For collisional plasmas, the cross-field electron diffusion coefficient is proportional to the frequency of collisions between electrons and other species in the plasma [14]. Thus, electron mobility in a HET is affected by the electron-neutral, electron-ion, and electron-wall collision frequencies. Once a given neutral is ionized its behavior is determined largely by its interaction with the local electric field. Thus, the anode temperature has a negligible impact on the ion-electron collision frequency. Equation (11) shows the electron-neutral collision frequency [15]. Since the electrons move much faster than the neutrals, the relative velocity between the electrons and the neutrals is approximately the average velocity of the electrons.

$$Z_c = n_0 Q_0 \bar{v}_{e0} \quad (11)$$

The collision cross section and electron velocity are independent of the neutral temperature [15]. Thus we can assume that the collision frequency will vary only with neutral density when the plasma temperature remains constant. Equation (12) gives the axial flux of Maxwellian particles [6]:

$$\Gamma = \frac{1}{4} n_0 \bar{v} = \frac{1}{4} n_0 \sqrt{\frac{8kT_0}{\pi m_0}} \quad (12)$$

Since the propellant flow rate remains constant between the cooled and uncooled thruster configurations, the axial flux of neutrals is constant by way of mass conservation. Constant  $\Gamma$  implies that the neutral density is inversely proportional to the square root of temperature. Thus, a reduction in anode temperature leads to an increase in the neutral number density, which increases the electron-neutral collision frequency. Based on the projected anode face temperatures (Fig. 8b), cooling yields an approximately 26.6% increase in the electron-neutral collision frequency. The cumulative effect of increased electron-neutral collision frequency is enhanced electron mobility and an increased electron flux to the anode. This contributes to the observed increase in discharge current when cooling is enabled, as seen in Table 1. Recall from Fig. 1 that the beneficial effects of cooling diminish as electron temperature increases. At the cooled 100 V operating conditions, the increases in efficiency and ion current density suggest that the increase in collision frequency due to cooling yields an increase in ionization fraction that outweighs the detrimental increase in electron current to the anode. Higher discharge voltage leads to elevated electron temperature, which increases the fraction of the electron population with sufficient energy to ionize the propellant. Thus, at voltages above 100 V there is little gain in ionization fraction due to cooling,

yet the discharge current increases due to the elevated electron-neutral collision frequency. The increased discharge current associated with cooling is sufficient to cause an overall decrease in efficiency above 100 V.

Contrary to expectation, the discharge current for the cooled 100 V, 10.0 mg/s test condition is lower than that of the corresponding uncooled condition. Daniel Brown studied the low discharge voltage behavior of a 6 kW laboratory model HET with characteristics similar to the P5 [16]. Brown identifies two distinct operating regimes that occur at low voltage, called the high-current mode and low-current mode. The low-current mode more closely resembles nominal thruster behavior, and the transition to the high-current mode becomes more prevalent as the propellant flow rate is increased. At a fixed propellant flow rate of 10 mg/s, Brown achieves transition to the high-current mode by sufficiently lowering the discharge voltage. The resultant increase in discharge current between 100 V and 200 V is approximately 20% with the 6 kW thruster. During the cooled and uncooled P5 tests at 100 V, 10 mg/s, the P5 transitions to the high-current mode. The transition is marked by a 22.2 and 24.8% increase in discharge current for the cooled and uncooled tests, respectively. Brown demonstrates that an increase in the neutral density in the channel will drive the thruster back toward the low-current regime, causing a decrease in discharge current. Based on these observations, the increase in neutral density caused by cooling the P5 anode partially mitigates the transition to the high-current mode. As a result, the cooled discharge current is slightly lower than the uncooled discharge current at this operating condition.

### Ionization Zone Length and Plume Properties

Reference [17] reports that elevated neutral temperature will lengthen the ionization zone and decrease the amplitude of the breathing mode oscillation. This is a manifestation of an increased penetration distance as described in Eq. (3). If cooling has the opposite effect, we might expect to see a contraction in the region of the ionization zone downstream of the radial magnetic field maximum. This could lead to greater collimation of the plume and increased discharge current oscillation amplitude. It is known from Fig. 13 that the discharge oscillation amplitude increases due to cooling, which contributes to the observed decrease in efficiency above 100 V. Table 2 suggests that cooling also causes an increase in the fraction of the total ion beam current contained within  $\pm 30^\circ$  of thruster centerline. These results are consistent with the data and theory presented in [17]. The improvement in beam collimation at discharge voltages above 100 V is not sufficient to affect a net increase in efficiency.

The current density profiles in Fig. 12 show that the cooled plume is consistently shifted off centerline in the angular direction of the propellant inlet tube. Reference [2] suggests that azimuthal nonuniformities in the plume are a likely mechanism for performance degradation. Because two thermocouples are used to measure the temperatures at the rear of the anode, it is known that thermal nonuniformities exist with and without cooling. Such thermal nonuniformities are, in part, caused by nonuniformities in the gas distribution pattern of the anode, which are in turn influenced by variations in the thermal expansion of the anode during thruster operation. In the design phase of this study, care was taken to ensure that the anode would be cooled uniformly. Despite these efforts, it is possible that cooling is somewhat nonuniform during testing. This would create variations in thermal expansion which could contribute to nonuniformities in the gas distribution as discussed above. Hot spots at the anode exit plane may facilitate a higher local propellant flow rate, which leads to greater electron flux in return. The enhanced electron flux would act to maintain or even exacerbate the hot spot. While the exact cause of the observed azimuthal nonuniformities is unknown, such nonuniformities are likely to contribute to the performance degradation measured herein.

Overall, the observed trends in performance are the result of a balance between the influences of ionization fraction, electron mobility, discharge oscillation amplitude, plume collimation, and propellant distribution. The changes in these parameters due to

cooling vary with the discharge voltage which results in gains in thrust and efficiency at 100 V, and losses at higher voltage.

### Conclusions

Neutral propellant temperature plays an important role in HET performance. Experimental data confirms that an increase in thrust and anode efficiency can be achieved by reducing the propellant temperature in the high  $T/P$  operating regime. The improvement in performance is driven by an increase in ionization fraction. The observed performance degradation associated with low neutral temperature at high discharge voltage is a manifestation of increased electron current to the anode, increased discharge current oscillation amplitude, and azimuthal nonuniformities caused by cooling, without any appreciable increase in ionization fraction. With an optimized anode design it may be possible to extend the positive effects of cooling to higher discharge voltages. Even so, the observed performance gains would still be maximized at low discharge voltage, where the fraction of the electron population with sufficient energy to ionize propellant is small.

The significant power consumption and mass of a forced convection cooling system would most likely render a cooled anode HET impractical for space operations. Alternatively, a passively cooled anode could potentially overcome these limitations. In general, this study reveals the importance of managing thermal energy in HETs and reinforces the value of optimized anode design, with special emphasis on maximizing propellant residence time and electron-neutral collision frequency for high  $T/P$  devices.

### References

- [1] Byers, D. C., and Dankanich, J. W., "Geosynchronous-Earth-Orbit Communication Satellite Deliveries with Integrated Electric Propulsion," *Journal of Propulsion and Power*, Vol. 24, No. 6, Nov.–Dec. 2008, pp. 1369–1375. doi:10.2514/1.35322
- [2] Reid, B., and Gallimore, A., "Review of Hall Thruster Neutral Flow Dynamics," 30th International Electric Propulsion Conference, IEPC Paper 07-038, Florence, Italy, Sept. 2007, pp. 2–13.
- [3] Wilbur, P. J., and Brophy, J. R., "The Effect of Discharge Chamber Wall Temperature on Ion Thruster Performance," *AIAA Journal*, Vol. 24, No. 2, Feb. 1986, pp. 278–283. doi:10.2514/3.9257
- [4] Haas, J. M., Gulczinski, F. S., III, Gallimore, A. D., Spanjers, G. G., and Spores, R. A., "Performance Characteristics of a 5 kW Laboratory Hall Thruster," 34th Joint Propulsion Conference, AIAA Paper 98-3503, Cleveland, OH, 12–15 July 1998.
- [5] COMSOL Multiphysics, Ver. 3.5a, COMSOL, Inc., Burlington, MA, Dec. 2008.
- [6] Goebel, D., and Katz, I., "Basic Plasma Physics," *Fundamentals of Electric Propulsion: Ion and Hall Thrusters*, Wiley, Hoboken, NJ, 2008, pp. 43–60.
- [7] Linnell, J., and Gallimore, A., "Internal Plasma Potential Measurements of a Hall Thruster Using Xenon and Krypton Propellant," *Physics of Plasmas*, Vol. 13, No. 093502, 1986, pp. 1–10. doi:10.1063/1.2335820
- [8] Hofer, R. R., "Development and Characterization of High-Efficiency, High-Specific Impulse Xenon Hall Thrusters," Ph.D. Dissertation, Dept. of Aerospace Engineering, Univ. of Michigan, Ann Arbor, MI, 2004, pp. 60–93.
- [9] Mazouffre, S., Echegut, P., and Dudeck, M., "A Calibrated Infrared Imaging Study on the Steady State Thermal Behaviour of Hall Effect Thrusters," *Plasma Sources Science and Technology*, Vol. 16, No. 1, 2007, pp. 13–22. doi:10.1088/0963-0252/16/1/003
- [10] Todreas, N. E., and Kazimi, M. S., "Single-Phase Heat Transfer," *Nuclear Systems Volume 1: Thermal Hydraulic Fundamentals*, Taylor and Francis, Washington, D.C., 1990, p. 443.
- [11] Xu, K. G., and Walker, M. L. R., "High-Power, Null-Type, Inverted Pendulum Thrust Stand," *Review of Scientific Instruments*, Vol. 80, May 2009, pp. 1–6. doi:10.1063/1.3125626
- [12] Rovey, J. L., Walker, M. L. R., Gallimore, A. D., and Peterson, P. Y., "Magnetically Filtered Faraday Probe for Measuring the Ion Current Density Profile of a Hall Thruster," *Review of Scientific Instruments*, Vol. 77, No. 13503, Jan. 2006, pp. 1–8. doi:10.1063/1.2149006
- [13] Walker, M. L. R., Victor, A. L., Hofer, R. R., and Gallimore, A. D., "Effect of Backpressure on Ion Current Density Measurements in Hall Thruster Plumes," *Journal of Propulsion and Power*, Vol. 21, No. 3, June 2005, pp. 408–415. doi:10.2514/1.7713
- [14] Chen, F. F., "Diffusion and Resistivity," *Plasma Physics and Controlled Fusion*, Vol. 1, 2nd ed., Springer-Verlag, New York, 2006, p. 172.
- [15] Jahn, R. G., "Ionization in Gases," *Physics of Electric Propulsion*, Dover, New York, 1996, pp. 46–60.
- [16] Brown, D. L., "Investigation of Low Discharge Voltage Hall Thruster Characteristics and Evaluation of Loss Mechanisms," Ph.D. Dissertation, Dept. of Aerospace Engineering, Univ. of Michigan, Ann Arbor, MI, 2009, pp. 260–300.
- [17] Furukawa, T., Miyasaka, T., and Fujiwara, T., "Methods of Controlling Low-Frequency Oscillation in a Hall Thruster," 27th International Electric Propulsion Conference, IEPC Paper 2001-057, Pasadena, CA, 15–19 Oct. 2001, pp. 5–8.

J. Blandino  
Associate Editor